

The behavior of iron under ultrafast shock loading driven by a femtosecond laser

S. I. Ashitkov, V. V. Zhakhovsky, N. A. Inogamov, P. S. Komarov, M. B. Agranat, and G. I. Kanel

Citation: **1793**, 100035 (2017); doi: 10.1063/1.4971660

View online: <http://dx.doi.org/10.1063/1.4971660>

View Table of Contents: <http://aip.scitation.org/toc/apc/1793/1>

Published by the [American Institute of Physics](#)

The behavior of iron under ultrafast shock loading driven by a femtosecond laser

S. I. Ashitkov^{1,a)}, V. V. Zhakhovsky², N. A. Inogamov³, P. S. Komarov¹,
M. B. Agranat¹ and G. I. Kanel¹

¹Joint Institute for High Temperatures, Russian Academy of Sciences, Moscow, 125412, Russia

²Dukhov Research Institute of Automatics, ROSATOM, Moscow 127055, Russia

³Landau Institute for Theoretical Physics, Russian Academy of Sciences, Chernogolovka, Russia

^{a)}ashitkov11@yandex.ru

Abstract. The results of experimental and theoretical investigations of shock-wave propagation in *bcc* iron under ultra-short loads driven by femtosecond laser pulses are presented. Chirped pulse interferometry was used for continuous diagnostics of movement in a picosecond range of the rear-side surface of thin iron films. The evolution of ultra-short elastic-plastic shock waves in samples with different thicknesses and purity has been studied. The obtained HEL and spall strength are close to ultimate values of shear and tensile stresses. Response of single-crystal iron to ultra-short shock loading/unloading was also explored in micron-sized films by molecular dynamics simulations. The experimental and simulation results on shock-induced elastic-plastic transformation and phase transition from *bcc* to *hcp* iron in a picosecond range of loading are discussed.

INTRODUCTION

Material response to ultra-short shock waves generated by femtosecond laser pulses (fsLP) has attracted considerable interest last decade. Recent experimental and theoretical studies of micrometer-sized metal films under ultra-short picosecond shear and tensile stresses demonstrated that materials can exhibit the very high shear and spall strengths closely approaching the corresponding theoretical ultimate mechanical properties [1–6]. Non-mechanical response of shocked materials, including non-equilibrium polymorphic phase transitions and melting, has also attracted the particular attention [7–9]. Extensive studies of material under ultra-fast compression and unloading can impact on the theories of phase transition, plasticity and strength of materials for such high strain rates. On other hand, progress in experimental techniques is required to check the results of atomistic simulation and two-temperature hydrodynamics modeling of metals irradiated by fsLP.

Here we present our recent results about behavior of sub-micron films of iron with different purity under ultra-short shock loading within a picosecond time scale. For diagnostics the ultra-fast chirped pulse interferometry is applied. This report supplements our preceding work [4] with new results. Molecular dynamics (MD) simulations of single-crystal iron films in conditions similar to those in experiments are also reported and compared with experimental data.

EXPERIMENTAL TECHNIQUE

Iron with the high purity of 99.99% was used for deposition of thin film on glass substrate with the help of magnetron sputtering method. In addition, we performed experiments with thin films made from armco iron with purity of 99.6%, which contains 0.021% of carbon, 0.13% of manganese and 0.15% of silicon. The thicknesses of iron films were measured to be 250 and 480 nm using atomic force microscope, while the glass plate was 150 μm thick.

Source of laser beam was a femtosecond Ti:S CPA laser system. Laser pump pulse was directed to the glass-iron interface through the glass substrate, while a probe pulse was sent to the free rear side of the iron film. Only a small part of chirped pulse with duration 300 ps was used for probing a target.

The incident fluence $F(x, y)$ of pump pulse has the Gaussian distribution on the target within a focal spot of $25 \mu\text{m}$ width at the level of e^{-1} . After each shot the target film was shifted to a new position by a three-coordinate micromanipulator.

Imaging Michelson interferometer in conjunction with the diffractive spectrometer Acton 2300i was applied for diagnostic of the movement of the rear surface. The used Fourier analysis of 2D interference patterns [10] combined with normalization of the phase distributions provides a small inaccuracy within 0.01 radian in the measured phase shift, which corresponds to an error in surface displacement in the range of 1 – 2 nm. The used experimental setup provides continuous record of target surface displacement as a function of time in the range of 0 – 200 ps with time resolution of 1 ps and spatial resolution of $2 \mu\text{m}$ in a plane of target. More details of experimental techniques can be found in [4].

EXPERIMENTAL RESULTS

Figure 1 shows the displacement $z(t)$ and velocity $u_{fs}(t)$ of free rear-side surface of samples made from $\text{Fe}_{99.99}$. Laser pulse with incident fluence $F_0 = 4 \text{ J/cm}^2$ and duration 200 fs irradiates the iron film with thicknesses 250 nm. While the surface displacement (black curve) was calculated directly from the phase shift measured in experiment, the surface velocity profile (blue curve) was obtained via differentiation of the dependence $z(t)$ with the subsequent iteration processing that ensures the best correspondence of the integral of the velocity (red curve) to the measured displacement profile. The error in the determination of the velocity was about 0.1 km/s.

The two-wave configuration of the arriving compression wave was determined from the velocity profiles shown on Fig. 1. The surface velocity u_{fs} associated with the first fast wave was 0.9 km/s in propagation of distance 250 nm.

The stress in uniaxially compressed material behind the elastic SW front can be calculated as $\sigma_{HEL} = \rho_0 U_S u_p$, which gives a magnitude of HEL equal to 23 GPa. Here we use the elastic shock Hugoniot in the form $U_S = c_l + 1.2u_p = 6.0 + 1.2u_p$, where $c_l = 6.0 \text{ km/s}$ is a longitudinal sound speed in iron at standard conditions from [4].

Figure 2 shows the similar displacement $z(t)$ and velocity $u_{fs}(t)$ profiles obtained after SW arrival to the rear-side surface of an armco iron film of 480 nm thick. It is found that the stress in an elastic precursor is $\sigma_{HEL} = 31 \text{ GPa}$ in this sample irradiated by fsLP with incident fluence $F_0 = 7 \text{ J/cm}^2$ and duration 800 fs.

Figure 3 shows a $P - V$ phase diagram of iron, where the obtained metastable elastic shock Hugoniot (red curve) is plotted. There are also the two equilibrium plastic Hugoniots of α - phase of low-pressure *bcc* iron (blue curve) and ϵ - phase of high-pressure *hcp* iron (green curve). The extension of plastic Hugoniot to metastable states of α - phase is shown by a dot-dashed blue line. A junction of α - Hugoniot and ϵ - Hugoniot at 13 GPa corresponds to the equilibrium polymorphic phase transition $\alpha \rightarrow \epsilon$.

The maximal shear stress was determined from difference of compressed state after elastic precursor front from a state on equilibrium Hugoniot of low-pressure solid phase with using the equation $4\tau/3 = \sigma_z(V) - p(V)$ from

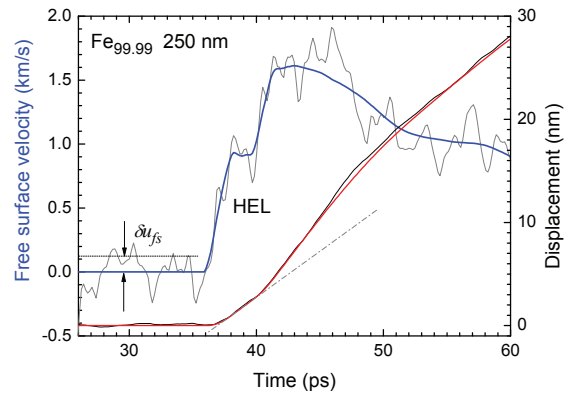


FIGURE 1. Displacement and velocity of free rear-side surface as functions of time after reflection of shock wave generated by fsLP with duration 200 fs and incident fluence $F_0 = 4 \text{ J/cm}^2$ for $\text{Fe}_{99.99}$ sample with thickness of 250 nm.

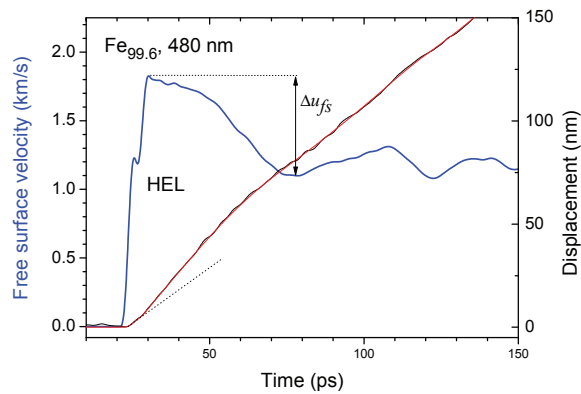


FIGURE 2. Displacement and velocity of free rear-side surface after reflection of shock wave generated by fsLP with duration 800 fs and incident fluence $F_0 = 7 \text{ J/cm}^2$ for $\text{Fe}_{99.6}$ sample with thickness of 480 nm.

[11], where σ_z is a longitudinal stress of elastic compression. It was found that the shear strength of $\tau = 7.0$ GPa measured in the high-purity iron film with thickness of 250 nm approaches the ultimate shear strength of 7.2–7.5 GPa obtained from *ab initio* calculations [12, 13]. Taking into account that elastic waves decay rapidly with increasing sample thickness at a micron scale [2, 4], the obtained data show that shear strength of the iron sample with purity of 99.6% is higher than one with purity of 99.99%

The spall strength, determined as a tensile stress just before fracture [4, 14], was measured from velocity pullback Δu_{fs} shown in Fig. 2. Because the plastic deformation of material occurs before formation of voids and cracks we use the following estimate of spall strength taking into account the elastic-plastic effects [15, 16]. In this case in the linear approximation for triangular shock profile the expression for the spall strength according to [15] gives an accuracy better 15% and has the form:

$$\sigma_{spall} = \rho_0 c_l \Delta u_{fs} / (1 + c_l / c_b) \quad (1)$$

However, accuracy of this equation for non-linear response of material to strong tensile stress at very high strain rate is controversial. As we will show in the next section, MD simulation indicates that Eq. (1) may lead to overestimation of the spall strength. For $\text{Fe}_{99.6}$ (Fig. 2) for the velocity pullback $\Delta u_{fs} = 0.73$ km/s the spall strength is found to be $\sigma_{spall} = 15$ GPa at the strain rate $\dot{V}/V \approx 10^9 \text{ s}^{-1}$.

Recently the polymorphic phase transition in iron was recognized in [8], where a relatively long laser pump pulse with duration of 300 ps and a sharp leading front was used. It was found that $\alpha \rightarrow \epsilon$ transition happens approximately 200 ps after HEL. The found stress of 25 GPa required for transition exceeds nearly twice the well-defined transition threshold of 13 GPa measured at low strain rates.

In contrast to [8] we did not find the $\alpha \rightarrow \epsilon$ transition in our experiments with ultrashort shock waves generated by fsLP. The realized shocked states in different iron films are shown on Fig. 3. All those states lie on either the elastic or plastic shock Hugoniot of low-pressure phase. Thus, the expected $\alpha \rightarrow \epsilon$ transition does not occur or an degree of transition is too small. Relying on molecular dynamics (MD) simulations discussed below, we think that the rapid unloading, happened about 50 ps after leading shock front, prevents development of such transition. MD results also indicate that to trigger such ultra-fast transition a much higher compression than we had is required.

SIMULATION RESULTS

MD simulation of laser-induced shock wave propagation in the free-standing iron films was performed with using a new EAM potential for iron developed in [17]. The potential was specifically fitted to reproduce bcc-to-hcp and bcc-to-fcc phase transitions in iron. While the film thickness of MD sample was identical to that in experiments, y - and z - dimensions were taken as $16.1 \times 16.2 \text{ nm}^2$ with periodic boundary conditions imposed along those axes. To obtain the single crystals with pre-existing dislocations the samples were initially subjected to a large shear deformation along y - axis. Then the samples were thermalized to $T = 300 \text{ K}$ with using the Langevin thermostat.

To mimic laser heating of the surface layer of a film the Langevin thermostat targeted at a Gaussian temperature profile with a heat depth of 45 nm was applied during 3 ps. Since the deposited energy was unknown in experiments the surface temperature of the Gaussian profile was varied in simulations to provide an amplitude of shock wave detected experimentally on the rear-side of film.

MD simulations of iron films oriented in the main crystallographic directions [100], [110], and [111] were performed. We found that the [100] is an exceptional direction, in which a laser-generated ultra-shot shock wave can easily trigger the $\alpha \rightarrow \epsilon$ transition as it is illustrated on Fig. 4. To recognize a kind of lattice during run-time of simulation the combined atomic order parameter $Q_4 - Q_6$ is used [17]. Molten material is colorized by purple, blue is used for *bcc* crystal, green for *hcp*, and red corresponds to *fcc* crystal.

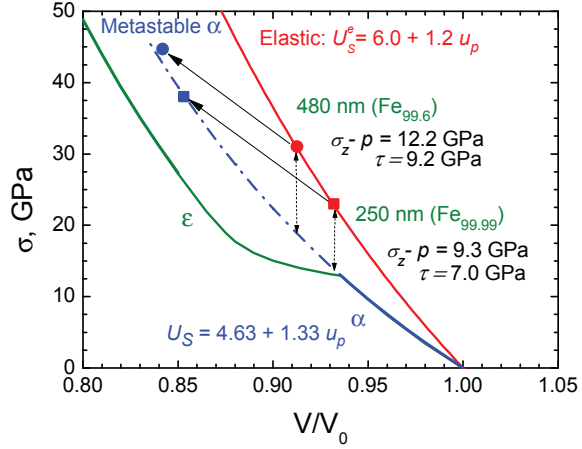


FIGURE 3. Phase diagram of iron in $P - V$ plane. Experimental data marked as squares are obtained for $\text{Fe}_{99.99}$ sample and circles corresponds to $\text{Fe}_{99.6}$ sample

The $\alpha \rightarrow \epsilon$ transition is initiated for very short time of 2-4 ps at the leading shock front where compression remains uniaxial in [100] direction. Under such deformation the (110) atomic planes of *bcc* crystal transform to 2D close-packed geometry similar to that in *hcp* lattice. The cooperative shuffle, described in [7], of many those planes produced by shear stress in the shock front results in transition of large domains to *hcp* structures as Fig. 4 illustrates.

Such fast transition relaxes the shear stress without notable motion and multiplication of pre-existed dislocations, i.e. without plastic deformation. The following uniaxial unloading in the tail of ultra-short shock-wave profile leads to the perfect reverse $\epsilon \rightarrow \alpha$ transition starting from $P_{xx} \approx 23$ GPa and completing at 13 GPa. As a result of such “perfect” direct and reverse phase transitions the temperature rises but little from 300 K in the uncompressed α -iron to 400 K in shocked ϵ -iron and 370 K in unloaded α -iron on the profile at 76.8 ps shown in Fig. 4. The temperature of 420 K was in shocked ϵ -iron at 38.4 ps. Such small shock heating is typical for strong elastic shock waves. After reflection of the shock pulse from the free rear-side surface the formed rarefaction wave produces tensile stresses, which may lead to spallation of a rear-side layer if the stress exceeds 16 GPa. This spall strength was taken directly from a simulated stress profile at the position of first void just before the moment of nucleation of this void. It can be done easily since we have full record of evolution of the simulated system.

It is worth noting that the use of Eq. (1) for estimating the spall strength from the simulated velocity of rear-side surface results in 23 GPa, which is about 40% higher than the calculated spall strength of 16 GPa. The similar error of about 25% was found in MD simulation of spallation in single-crystal gold films [18]. Thus, Eq. (1) substantially overestimates the spall strength calculated in MD simulation of spallation by an ultrashort laser pulse.

In contrast to [100] crystallographic direction, it was found that the ultra-short shock waves propagating in [110] and [111] directions should have much higher pressure to induce the $\alpha \rightarrow \epsilon$ transition because the shuffle mechanism is not directly applicable in those directions of compression. Like in the above-discussed experiments our simulation indicates no such transition within the attenuated shock wave profiles approaching the rear-side surface of film after propagation of 540 nm. However, this transition is found to happen during the early stage of propagation when the shock pressure is large enough. Figure 5 shows that at higher compression in an ultra-short shock wave entering from the heated frontal layer the $\alpha \rightarrow \epsilon$ transition is realized (at least partially in several spots), but in an attenuated shock

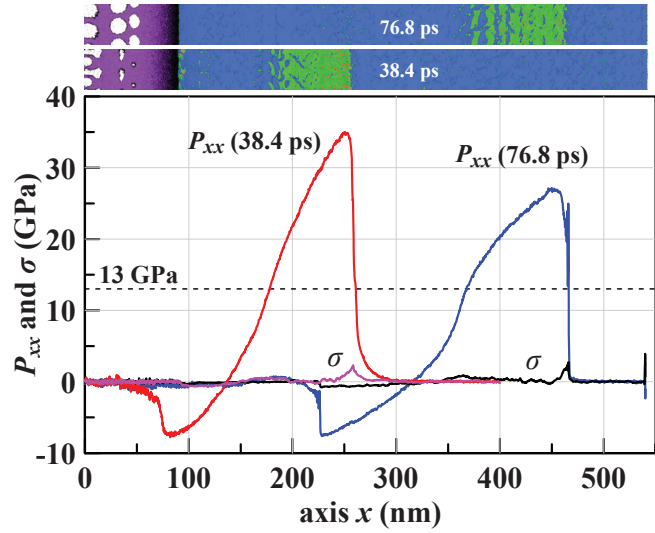


FIGURE 4. Snapshots of combined atomic order parameter $Q_4 - Q_6$ and stress $P_{xx} \equiv -\sigma_{xx}$ profiles in a single-crystal iron film oriented in $x = [100]$. Molten material is colored by purple, *bcc* crystal – blue, *hcp* – green, and red corresponds to *fcc* crystal. $\alpha \rightarrow \epsilon$ transition occurs just after elastic zone. The reverse $\epsilon \rightarrow \alpha$ transition starts from $P_{xx} \approx 23$ GPa and completes at 13 GPa on the unloading tail of ultra-short shock-wave profile.

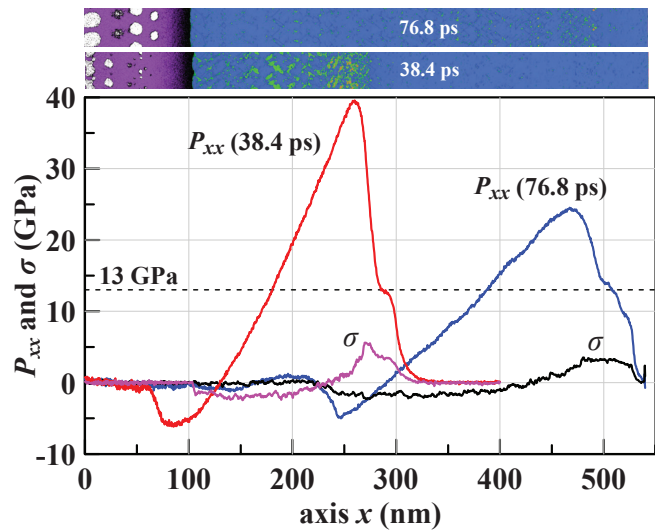


FIGURE 5. Snapshots of combined atomic order parameter $Q_4 - Q_6$ and stress profiles in a single-crystal iron film oriented in $x = [110]$. $\alpha \rightarrow \epsilon$ transition can occur at high-pressure shock in early stage of propagation. The reverse $\epsilon \rightarrow \alpha$ transition happens on the unloading tail of ultra-short shock within $P_{xx} = 10 - 13$ GPa. After drop of shock stress below 30 GPa the $\alpha \rightarrow \epsilon$ stops.

$P_{xx} < 30$ GPa this transition ceased, which is in a agreement with above experimental results (see Fig. 3). Because crystalline domains are oriented incidentally in experimental samples the peculiar behavior of [100] oriented domains, found in our MD simulation, play a negligible role in response of polycrystal to shock-wave loading/unloading in our experiments.

CONCLUSION

Ultrafast single shot interferometric diagnostics using a chirped laser probe was implemented to measure surface displacement of target with accuracy of 1–2 nm. This technique was used to study response of iron film to ultrashort shock wave loading produced by femtosecond laser irradiation. We have found that uniaxial shock compression in iron at the submicron scale is elastic up to 31 GPa. MD simulation shows the maximal stress of 30 GPa can be achieved in an elastic shock wave in early stage of propagation. The measured shear stress of 7.0 GPa in picosecond range of loading is close to the ultimate shear strength of iron [12, 13], while the shear stress observed in MD simulation of super-elastic shock wave is about 7.6 GPa for propagation along [110] direction and 10.7 GPa for [111] direction.

Our experiments reveal that the polymorphic $\alpha \rightarrow \epsilon$ phase transition in polycrystalline iron film of 480 nm thick is not realized at a stress of 45 GPa within 50 ps after HEL. On the other hand our MD simulation of [110] and [111] oriented single-crystal films shows that the $\alpha \rightarrow \epsilon$ transition may happen at the experimental conditions within only first 100-200 nm of film where the shock stress exceeds 30 GPa.

By contrast in the [100] oriented single crystal the transition is easily produced by an elastic shock with stress exceeding 23 GPa. This transition is not associated with dislocation dynamics and also perfectly reversible in the unloading part of [100] shock wave profile, where it is initiated at stress of 23 GPa. For all other orientations the reverse $\epsilon \rightarrow \alpha$ transition is initiated at about 13 GPa in the unloading tail.

ACKNOWLEDGEMENTS

In this work the experimental research (S.I.A, P.S.K, M.B.A, G.I.K) was supported by Rosatom (GK H4x.44.90.13.1111) and MD simulation (V.V.Z and N.A.I) by the Russian Science Foundation (project No. 14-19-01599).

REFERENCES

- [1] S. I. Ashitkov, M. B. Agranat, G. I. Kanel', P. S. Komarov, and V. E. Fortov, *JETP Lett.* **92**, 516–520 (2010).
- [2] V. H. Whitley, S. D. McGrane, D. E. Eakins, C. A. Bolme, D. S. Moore, and J. F. Bingert, *J. Appl. Phys.* **109**, p. 013505 (2011).
- [3] J. C. Crowhurst, M. R. Armstrong, K. B. Knight, J. M. Zaugg, and E. M. Behymer, *Phys. Rev. Lett.* **107**, p. 144302 (2011).
- [4] S. I. Ashitkov, P. S. Komarov, M. B. Agranat, G. I. Kanel', and V. E. Fortov, *JETP Lett.* **98**, 394–400 (2013).
- [5] B. J. Demaske, V. V. Zhakhovsky, N. A. Inogamov, and I. I. Oleynik, *Phys. Rev. B* **87**, p. 054109Feb (2013).
- [6] S. I. Ashitkov, N. A. Inogamov, P. S. Komarov, V. V. Zhakhovsky, I. I. Oleynik, M. B. Agranat, G. I. Kanel, and V. E. Fortov, *AIP Conference Proceedings* **1464**, 120–125 (2012).
- [7] K. Kadau, T. C. Germann, P. S. Lomdahl, and B. L. Holian, *Phys. Rev. B* **72**, p. 064120 (2005).
- [8] J. C. Crowhurst, B. W. Reed, M. R. Armstrong, H. B. Radousky, J. A. Carter, D. C. Swift, J. M. Zaugg, R. W. Minich, N. E. Teslich, and M. Kumar, *Journal of Applied Physics* **115**, p. 113506 (2014).
- [9] M. M. Budzevich, V. V. Zhakhovsky, C. T. White, and I. I. Oleynik, *Phys. Rev. Lett.* **109**, p. 125505 (2012).
- [10] V. V. Temnov, K. Sokolovski-Tinten, and P. Zhou, *J. Opt. Soc. Am. B* **23**, p. 1954 (2006).
- [11] Y. B. Zel'dovich and Y. P. Raizer, *Physics of Shock Waves and High-Temperature Hydrodynamic Phenomena* (Dover, 2002).
- [12] D. M. Clatterbuck, D. C. Chrzan, and J. W. Morris, *Acta Materialia* **51**, p. 2271 (2003).
- [13] S. Ogata, J. Li, N. Hirotsaki, Y. Shibutani, and S. Yip, *Phys. Rev. B* **70**, p. 104104 (2004).
- [14] S. Eliezer, E. E. Moshe, and D. Eliezer, *Laser and Particle Beams* **20**, p. 87 (2002).
- [15] G. I. Kanel, *J. Applied Mechanics and Technical Physics* **42(2)**, p. 358 (2001).
- [16] G. I. Kanel, *Int. J. Fract.* **163**, p. 173 (2010).
- [17] V. V. Zhakhovsky, K. P. Migdal, N. A. Inogamov, and S. I. Anisimov, AIP Conference Proceedings (2016), in this Proceedings.
- [18] B. Demaske, V. V. Zhakhovsky, N. A. Inogamov, and I. I. Oleynik, *Phys. Rev. B* **82**, p. 064113 (2010).